An effective design strategy of small bipolar molecules through fused conjugation towards 2.5 V based redox flow batteries

Yue Liu,[a,b,+] Gaole Dai,[c,+] Yuanyuan Chen,[a] Ru Wang,[a] Huamei Li,[a] Xueliang Shi,[d] Xiaohong Zhang,*[a] Yang Xu*[b] and Yu Zhao*[a,c]

[a] Institute of Functional Nano & Soft Materials (FUNSOM), Jiangsu Key Laboratory for Carbon-based Functional Materials & Devices, Soochow University, 199 Renai Road, Suzhou, Jiangsu 215123, P.R. China, E-mail: xiaohong_zhang@suda.edu.cn

[b] Department of Chemistry, University College London, 20 Gordon Street, London, WC1H 0AJ, UK, E-mail: y.xu.1@ucl.ac.uk

[c] College of Materials, Chemistry and Chemical Engineering, Hangzhou Normal University, 2318 Yuhangtang Road, Hangzhou, Zhejiang 311121, P.R. China, E-mail: yuzhao@hznu.edu.cn

[d] Shanghai Key Laboratory of Green Chemistry and Chemical Processes, School of Chemistry and Molecular Engineering, East China Normal University, 500 Dongchuan Road, Shanghai 200062, P.R. China

[+] These authors contribute equally.

Abstract:

Using bipolar redox-active molecules (BRMs) as active materials is a practical way to address electrolyte crossover and resultant unpredictable side reactions in redox-flow batteries. However, the development of BRMs is greatly hurdled by difficulties in finding new molecules from limited redox-active moieties, and in achieving high cell voltage to compete with existing flow battery chemistries. This study proposes a strategy for design of high voltage BRMs using fused conjugation that regulates the redox potential of integrated redox-active moieties. As a demonstration, quaternary N and ketone redox moieties are used to construct a new BRM that shows prominent voltage gap with good electrochemical stability. A symmetric redox-flow cell based on this molecule exhibits high voltage of 2.5 V and decent cycling stability. This study provides a general strategy for designing new BRMs that may enrich the cell chemistries of organic redox flow batteries.

TOC graphic

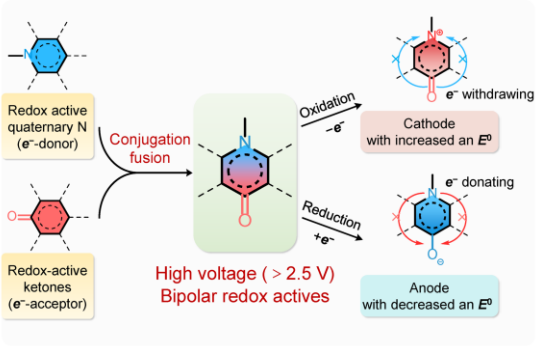

Redox flow batteries (RFBs) are considered a promising storage technology for grid-scale electrical energy storage due to the flexibility of configuring cells and the ability to decouple power and energy density in comparison to other battery technologies using solid electrodes. [1-3] Although RFBs have received a remarkable improvement in the past a few decades, obstacles such as relatively low energy density and electrolyte crossover need to be addressed before proceeding to practical implementation. [4-6] On the one hand, non-aqueous solvents are preferable over aqueous counterparts to improve energy density, because the former has a broader electrochemical potential window than the latter, which is essential for the cell to reach a high output voltage. [7-9] Moreover, a great number of non-aqueous soluble redox-active organic molecules (ROMs) significantly broaden the range to choose active materials. Benefit of using ROMs as active materials arises from their elemental sustainability, structural diversity and more importantly, structural tunability that is the key to enhance the (electro)chemical stability and tailor the redox potential of RFBs via the molecular engineering strategies. [10-13] On the other hand, crossover can cause electrolyte contamination, which inevitably lowers the utilization ratio of active materials and may trigger unpredictable side reactions between electrolyte constituents. [14]

A practical way to address the above challenges is to use bipolar redox-active molecules (BRMs). They are different from traditional ROMs, because they can be either oxidized to a positively charged state or reduced to a negatively charged state, with the feature of both reduction and oxidation reactions being independent and reversible. [15] As a result, the two half compartments of an RFB can utilize same redox-active molecule and electrolyte, i.e., a symmetric RFB. [16,17] This configuration can mitigate the challenge of crossover by eliminating the chemical concentration gradient in the discharge state. [18] Even

if the charging species permeate across the separator during cell operation, a symmetric RFB can return to its initial state to avoid permanent degradation caused by internal shuttle effect, which can theoretically extend cell lifetime and enhance the utilization efficiency of BRMs. [17,19] Beneficial from these remarkable characteristics, symmetric RFBs hold great prospects for grid-scale electrical energy storage. So far, several strategies have been developed to construct symmetric RFBs, including forming bipolar eutectic mixtures (Figure S1a), [20-23] combining different redox-active moieties through covalent bonding (Figure S1b), [24-27] and physically mixing anode- and cathode-active molecules to form an electrolyte (Figure S1c). [28,29] Although these strategies are highly promising in addressing the challenge of electrolyte contamination, they all have obvious weaknesses. Bipolar eutectic mixtures generally exhibit a high viscosity that significantly reduces the diffusion rate of active molecules, so the resulting electrolytes could only be operated at a relatively low current density. [30,31] Both physically mixed redox-active moieties and covalently bonded anode- and cathode-active molecules would not change the electrochemical characteristics of origin redox-active moieties, while, complicate fabrication procedures and raises manufacturing cost. [32-34] Furthermore, current studies on BRMs are limited by the fact that BRMs are composed of previously known redox-active molecules or their combinations, and BRMs that are capable to deliver an output voltage greater than 2.5 V are yet to be demonstrated. [27,35-39] Therefore, it's highly desirable to develop fundamentally new BRM structures with high output voltage and regulable electrochemical characteristics with utmost compatibility to non-aqueous RFBs.

Electrochemical characteristics of ROMs are directly determined by the electron density distribution around the redox-active moiety and can be regulated by incorporating electron withdrawing and donating

groups into the molecules. [40] As known, *p*-type molecules are regarded as electron donors because they prefer losing electrons in redox reactions, whereas *n*-type molecules are regarded as electron acceptors because they prefer gaining electrons in redox reactions. [41] When a *p*-type moiety and a *n*-type moiety are sufficiently close to each other, at which they are fused to a larger extent through conjugation sharing, [42] it is possible to simultaneously and synergically regulate redox potentials of the moieties due to the direct electronic perturbation between them and form a new type BRMs. In this study, we prove effective a general design strategy of BRMs by fusing *p*- and *n*-type redox moieties in a same conjugated structure through synergized electron delocalization and inductive effects. As a demonstrator, we prepared a BRM, 11-methoxy-9*H*-quinolino[3,2,1-*kl*]phenothiazin-9-one, denoted as QPT-OMe, and applied it as both anode and cathode materials for a symmetric RFB. The battery delivers an impressive discharge voltage of ~2.5 V, which is superior to most of the reported symmetric RFBs based on BRMs. Moreover, density functional theory (DFT) study reveals that compared with the pristine *p*- and *n*-type moiety, QPT-OMe shows an extended conjugation that enables sufficient charge delocalization and stable intermediates in the redox reactions. [43] In addition to the enhanced discharge voltage, our design strategy of BRMs eliminates the weaknesses of previous strategies and the issue of electrolyte crossover in conventional RFBs. We believe the strategy might open a new avenue to design BRMs and in a wide sense benefit the performance improvement of RFBs.

Figure 1a illustrates our design strategy of BRMs by using quaternary N (electron donor) and ketone (electron acceptor) as the redox-active moieties because they have been widely adopted in organic batteries and RFBs. Upon conjugation fusion, the molecular orbital would be reorganized compared with

each individual redox-active moiety. Once fusing the two redox-active moieties into the same conjugation, the electron density around the N atom is reduced due to the electron-withdrawing effect from the para-ketone moiety, while the electron density around the ketone moiety is increased due to the electron-donating effect from the para-quaternary N that possesses a lone pair electron in the p-orbital perpendicular to the conjugated plane. [44,45] When an oxidation reaction occurs, a higher potential is needed to remove one electron from the *p* orbital of N because negative charge compensation is obstructed by the presence of the electron-withdrawing ketone moiety, resulting in an increase in oxidation voltage. Similarly, when a reduction reaction occurs, a lower potential is needed for the ketone moiety to gain one electron because negative charge compensation is contributed by the presence of the electron-donating quaternary N moiety, resulting in a decrease in reduction voltage. As a result, when such kind of BRM is used as both cathode and anode materials in a symmetric RFB, the potential separation of the two half reactions is enlarged; hence, the output voltage of the RFB is increased and the intermediates of the BRM could be stabilized by the intensified electron delocalization.

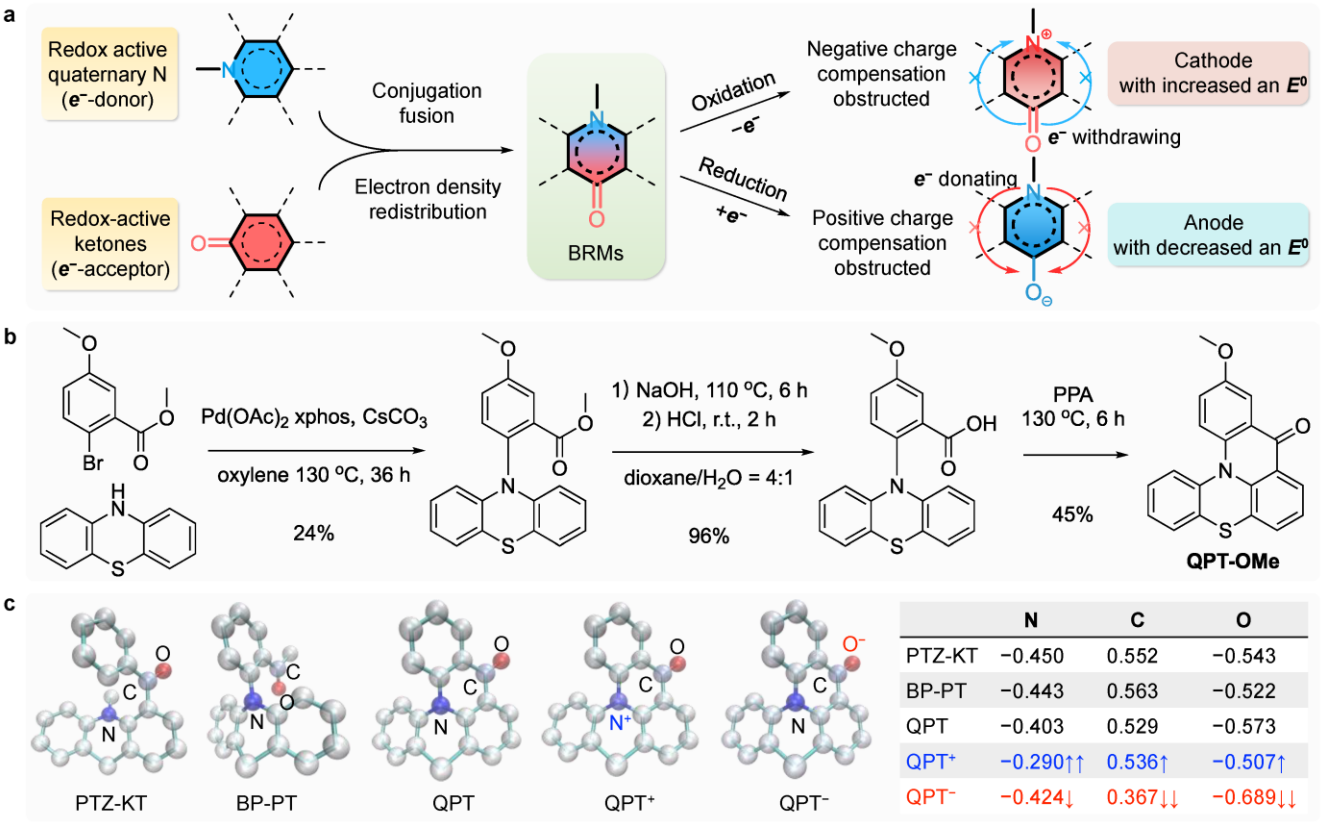

Figure 1. Design strategy, synthesis and electron density redistribution in selected BRMs with fused conjugation. a) Molecular design strategy of BRM using quaternary N and ketone as the redox-active moiety. b) Synthetic routs for QPT-OMe; c) NPA study of electron density redistribution in PTZ-KT, BP-PT, QPT and its redox intermediates. The NPA charge of other atoms is not shown for clarity.

Based on this strategy, we designed the molecule of QPT-OMe by fusing ketone as the electron-withdrawing moiety and quaternary N as the electron-donating moiety into a conjugation system. As shown in Figure 1b. QPT-OMe was synthesized using inexpensive and commercially available methyl 2-bromo-5-methoxybenzoate and 10*H*-phenothiazine through Pd-catalyzed coupling, followed by acidification reaction after hydrolysis and intramolecular acylation effecting cyclization (see synthetic procedures in Supporting Information). In addition, in order to achieve a high solubility in a non-aqueous

electrolyte [46], an ether chain was grafted to the QPT core (see synthetic procedures in Supporting Information) and the obtained BRM, (11-(2-(2-(2-methoxyethoxy)ethoxy)ethoxy)-9*H*-quinolino[3,2,1-*kl*]phenothiazin-9-one (denoted as QPT-TEG), was a viscose fluid and miscible with many polar organic solvents (Figure S2).

We examined the electron density distribution around the orthonormal natural atomic orbitals in the QPT core and the redox intermediates $QPT^{\bullet+}$ (upon oxidation) and $QPT^{\bullet-}$ (upon reduction) by NPA, which is an effective way to describe the electron distribution in compounds of high ionic character with improved numerical stability,[47] and compared with two similar structures, (10-methyl-10*H*-phenothiazin-1-yl)(phenyl)methanone) and 1-(2-(10*H*-phenothiazin-10-yl)phenyl)ethan-1-one (denote as "PTZ-KT" and "BP-PT"), without fused conjugation (Figure 1c, the values of NPA charges are provided in Table S1). Compared with PTZ-KT and BP-PT, QPT-OMe showed a greater NPA charge value in the quaternary N and a lower NPA charge value in C and O of ketone, suggesting that the fused conjugation promotes the electron density to redistribute from the electron-rich quaternary N moiety to the electron-deficient ketone moiety. Furthermore, in both cases of $QPT^{\bullet+}$ and $QPT^{\bullet-}$, the NPA charge values of N, C and O both increased upon oxidation, where a large increase was found in the quaternary N, implying that the negative charge transfer from C=O to N^+ is obstructed. Similarly, the NPA charge values of N, C and O both decreased upon reduction, suggesting that the positive charge transfer from quaternary N to $C\text{-}O^-$ is obstructed. Therefore, the oxidation potential of quaternary N is increased and the reduction potential of C=O is decreased in QPT comparing with the other two structures, resulting in a broadened voltage gap between the two redox moieties. Such a charge transfer was further

experimentally confirmed by excluding the influences from the electron-donating quaternary N and electron-withdrawing C=O (Figure S3).

Frontier molecular orbital theory was then used to validate the redox centers on QPT. As known, for *n*-type redox centers, a higher energy level of lowest unoccupied molecular orbital (LUMO) indicates a weaker electron affinity and a lower redox potential. For *p*-type redox centers, a lower energy level of highest occupied molecular orbital (HOMO) indicates a stronger electron affinity and a higher redox potential. [42,48] As shown in Figure S4, the calculated HOMO energy level of QPT was significantly lower than those of PTZ-KT and BP-PT. Noted that QPT showed a moderate LUMO energy level that was slightly lower than that of BP-PT, because the benzene ring of BP-PT has a high rotational degree of freedom, which can promote the conjugation integration with the ketone moiety, increasing the LUMO energy level. Nevertheless, QPT exhibited the broadest energy gap that would translate to the largest potential separation the oxidation and reduction reactions. Besides, the HOMO and LUMO energy levels of QPT and its derivatives (Figure S5) distributed exclusively on the quaternary N (oxidation reaction) and ketone moieties (reduction reaction), respectively. And the same molecular orbital energy level demonstrating same characteristics of three derivatives. Moreover, we calculated the HOMO and LUMO energy levels of other BRMs following a same design strategy (Figure S6), and found that the potential difference between *p*-type and *n*-type redox-active moieties can be readily broadened in a fused conjugation. This further validates the rationale of our strategy. In summary, the theoretical investigations confirmed that fused conjugation is a simple yet effective way to increase the voltage gap of BRMs.

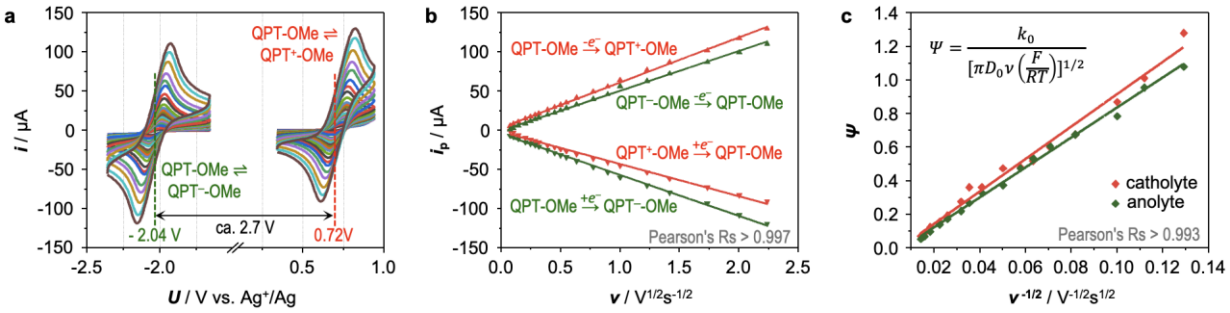

Figure 2. CV study of the redox kinetics of QPT-OMe. a) CV profiles of an acetonitrile solution composed 2 mM QPT-OMe and 100 mM TBA-TFSI at various sweeping rate from 5-5000 mV s^{-1}; b) Plots of anodic and cathodic peak currents (i_p) versus the square root of the sweeping rate ($v^{1/2}$) derived from the CV profiles; c) Plots of kinetic parameter, Ψ, versus reciprocal of the square root of the sweeping rate ($v^{-1/2}$). The expression of Ψ is shown in the upper right equation. Ψ is a dimensionless kinetic parameter, which is dependent on v, diffusion coefficient (D_0) and electron-transfer rate constant (k_0) of the electroactive species. F, R and T represent the Faradic constant, gas constant and absolute temperature, respectively.

Redox kinetics of QPT-OMe was investigated by cyclic voltammogram (CV) using tetrabutylammonium bis(trifluoromethylsulfonyl)imide (TBA-TFSI) in acetonitrile as the electrolyte. As shown in **Figure 2a**, two pairs of symmetric cathodic and anodic peaks are clearly observed. The half-wave potentials at −2.04 and 0.72 V (vs. Ag^+/Ag) correspond to the reduction and oxidation reactions of QPT-OMe, respectively. Accordingly, the open-circuit voltage when using QPT-OMe as the active material in RFBs is estimated to be ca. 2.76 V, which is one of highest voltage of bipolar molecules so far. [33,34] Notably, cathodic and anodic peaks remained highly symmetric across a wide sweeping rate

between 5 and 5000 mV s^{-1}. A good linear relationship can be found between peak current and the square root of sweeping rate (**Figure 2b)**, indicating the redox reactions are diffusion-controlled. [49] The diffusion coefficient (D_0) of QPT-OMe was calculated to be 2.3×10^{-6} cm^2 s^{-1} by using the Randles-Sevcik equation. The electron transfer rate constant (k_0) was also calculated according to Nicholson's analysis [50] shown in **Figure 2c**. Impressively, QPT-OMe/$QPT^{\bullet-}$-OMe and $QPT^{\bullet+}$-OMe/QPT-OMe redox couples showed an electron-transfer rate constant of 1.4×10^{-2} and 1.6×10^{-2} cm s^{-1}, respectively. This is because an outer sphere one-electron transfer from or to an aromatic π system requires a relatively low energy of reorganization. [39] Such high diffusion coefficient and electron transfer rate constant may favor to achieve better cell performance, particularly in minimizing the voltage hysteresis. [51] In addition, we carried out CV test on a mixture of QPT-OME and QPT-TEG. The waveform of the two BRMs was overlapped completely (Figure S7), demonstrating that functionalization with polar groups is a readily and effectively accessible method to enhance energy density, without severely changing the redox behavior and electronic configuration of the QPT core.

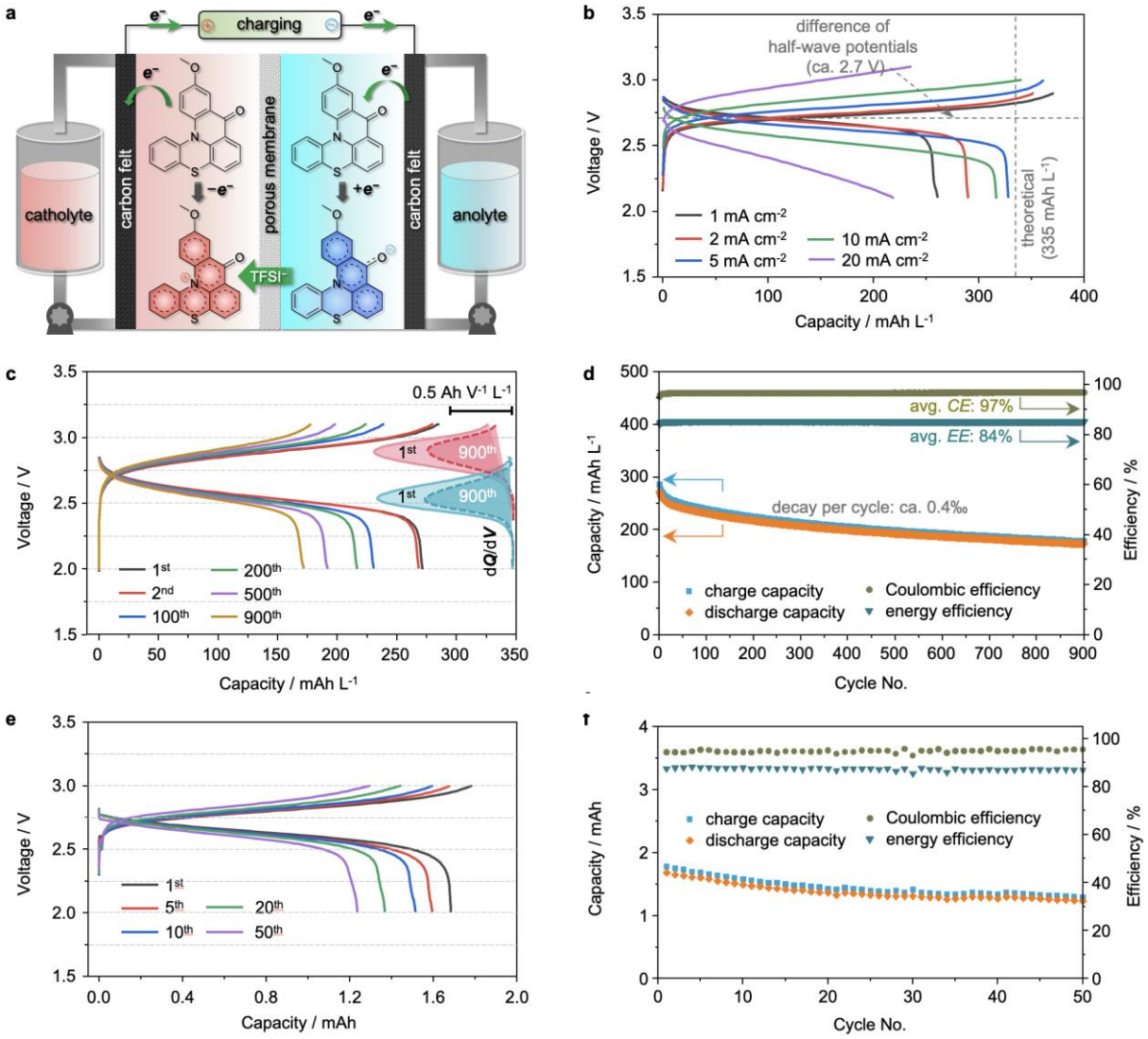

Figure 3. Galvanostatic charge-discharge behavior of symmetric RFB based on QPT-OMe. a) Cell architecture and the electrochemical processes during cell charging; b) Representative charge-discharge profiles at different current density; c) Selected charge-discharge profiles during long-term cycling; (d) Corresponding capacity retention, CE and EE of a non-flow cell. The non-flow cell was evaluated at constant current density of 5 mA cm^{-2} with equal volume of 0.1 mL 25 mM QPT-OMe and 0.5 M TBA-TFSI in acetonitrile as the electrolyte; (e) Representative charge-discharge profiles during long-term cycling; (f) Corresponding capacity retention, CE and EE of flow cell. The flow cell was evaluated at

constant current density of 10 mA cm^{-2} with equal volume of 3 mL 25 mM QPT-OMe and 0.5 M TBA-TFSI in acetonitrile as the electrolyte.

To verify the feasibility of QPT-OMe as an active material in a symmetric non-flow cell, an acetonitrile solution containing QPT-OMe and TBA-TFSI was used as both catholyte and anolyte, and a porous membrane was used as the separator. Cell architecture and electrochemical processes are illustrated in **Figure 3a**. The cathode and anode compartments of the cell were injected with an equal volume of 0.1 mL 0.025 M QPT-OMe in a 0.5 M TBA-TFSI/acetonitrile solution with a theoretical capacity of 335 mAh L^{-1}. Typical charge/discharge profiles shown in **Figure 3b** exhibited distinct charge/discharge plateaus at all measured current densities. At a low current density (< 5 mA cm^{-2}), the discharge voltage was 2.5−2.7 V with relatively small voltage hysteresis. To our knowledge, one of the highest values for RFBs. [31,36,37,52] The utilization ratio of QPT-OMe at the current densities of 1, 2, 5, 10 and 20 mA cm^{-2} were 77.6, 86.3, 97.6, 94.3, and 65.4% with the corresponding Coulombic efficiencies (CE)s of 70.0, 82.1, 90.6, 92.9, and 92.8%, respectively. The internal shuttle effect caused by a porous ion-conductive membrane may be responded to the “overcharge” phenomenon. The utilization ratio and the corresponding Coulombic efficiency kept increasing with the increase of current density below 5 mA cm^{-2}. The reason should be resulted from the alleviation of internal shuttle effect as the shortened of charge-discharge time. [53] Meanwhile, at a higher current density (> 10 mA cm^{-2}), the cell showed more obvious voltage hysteresis due to the concentration polarization that limits the mass transport in the electrolyte and across the separator, causing utilization ratio and CE decreased at the current density of 20 mA cm^{-2}. **Figures 3c** and **3d** show the charge-discharge profiles after different

cycles and long-term capacity retention of the symmetric cell. Voltage plateau remained almost unchanged for 900 cycles. This is further proven by the differential capacity analysis shown in the right panel of **Figure 3c,** where the potential range of charging (2.7-3.1 V) and discharging processes (2.4-2.7 V) as well as peak positions showed no change during the long-term cycling, suggesting the capacity was solely contributed by the discussed redox reactions. Capacity retention was ca. 63.5% after 900 cycles with a decay rate of ca. 0.4‰ per cycle, and CE and energy efficiency (EE) reached ca. 97% and 84%, respectively. The presented performance is superior to most non-aqueous RFBs either using BRMs or asymmetric organic molecules as active materials. [31,36,37,52]

We further tested the electrochemical performance of QPT-OMe in a flow cell (Figure S8). It exhibited similar charge/discharge profiles as those of the non-flow cell, shown in **Figure 3e** with utilization ratio of QPT-OMe of ca. 83.5% and capacity retention of 73.8% after 50 cycles. The corresponding CE and EE reached 95% and 87%, respectively as demonstrated in **Figure 3f**. The satisfactory structural stability of QPT-OMe could be further demonstrated by the almost identical CV profiles of the leachates of anolyte and catholyte after cycling (Figure S9). The capacity decay may arise from unpredictable side reactions, such as the carbonyl-based radical with acetonitrile through either nucleophilic substitution [54,55], increased internal resistance (Figure S10) caused by surface oxidation of carbon felt at high oxidation potential (1.4 V vs. NHE), and possible precipitation and deactivation of trapped active materials in porous graphite plate as a result of solvent evaporation. [56,57] Moreover, a symmetric non-flow cell with a higher concentration was examined by using QPT-TEG owing to its higher solubility than QPT-OMe. Figure S11 shows the charge/discharge profiles at diffident cycles,

where the voltage plateaus maintained at ca. 2.3 V upon discharging. The utilization rate of the active material in the first cycle was 74.6%, and the discharge capacity remained 63% after 200 cycles (Figure S12). Compared to the cell with low concentration, both the active material utilization and capacity retention declined, which is a common phenomenon in RFBs using concentrated electrolyte. Because both electrolyte viscosity and mass transfer polarization increased with the increase of active material concentration. [58,59] Besides, we performed the CV (Figure S13) and cycling test (Figure S14) of the QPT-TEG with different solvents. On the whole, QPT based molecules exhibited the best performance when use acetonitrile as electrolyte solvent.

The capability of QPT-OMe as a BRM was further confirmed in a pole reversal experiment with a non-flow cell, where the polarity of the cell was reversed every 50 cycles for 200 cycles, followed by another 300 cycles without being reversed. The charge/discharge profiles (**Figure 4a** and **4b**) exhibited a high symmetry throughout the entire cycling process, and no deviations can be observed between two consecutive periods of charging or discharging. The capacity retention reached ca. 56% after 500 cycles, and CE and EE remained at a high level of ca. 94 and 86%, respectively, as indicated in **Figure 4c**. It is worth noting that charge and discharge capacities increased initially after a pole switch and were stabilized after a few cycles. This is ascribed to the fact that an additional capacity was sacrificed to balance the remained $QPT^{\bullet+}$-OMe and $QPT^{\bullet-}$-OMe in the prior cycle in the catholyte and anolyte, respectively, resulting in a sudden drop of both CE and EE. As the cycling continued, the rebalancing of the whole battery system by continued pole reversals would alleviate such a capacity increase and reach a steady state. The results shown in Figures 3 and 4 demonstrated the good stability and chemical

reversibility of QPT-OMe. Compared with previously reported BRMs (summarized in Table S2), QPT-OMe delivered not only one of the highest output voltages (2.5 V) so far, but also a low molecular weight, which lead to an energy density of 202 W h kg^{-1} compared with those typically less than 150 W h kg^{-1}. [8,16,17,39,60-64]

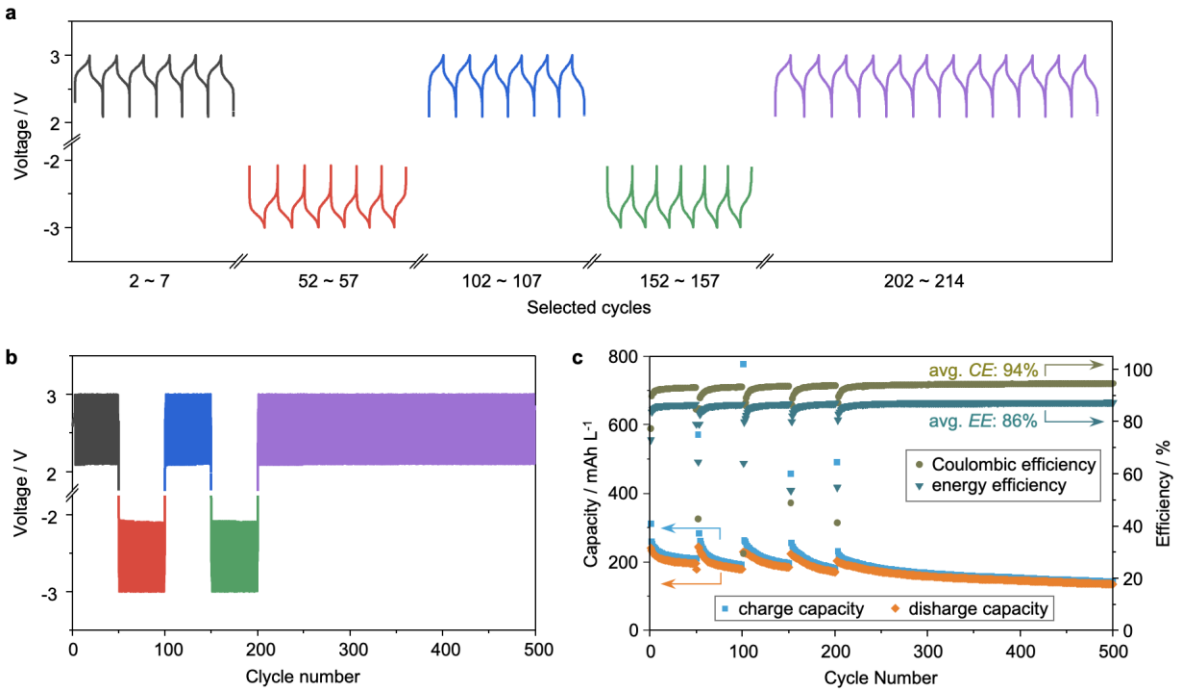

Figure 4. Pole reversal experiment of QPT-OMe in a symmetric cell. a) Representative galvanostatic charge/discharge profiles and b) long-term battery cycling of the polarity reversal experiment. c) Corresponding charge/discharge capacity, CE and EE. The no-flow cell is evaluated at a current density of 5 mA cm^{-2} with equal volume of 0.1 mL 25 mM QPT-OMe and 0.5 M TBA-TFSI in acetonitrile as the electrolyte. The polarity of the cell was reversed after each 50 cycles for 4 times, and then kept cycling for another 300 times.

Furthermore, temporal three-electrode spectroelectrochemical X-band electron paramagnetic resonance (EPR) [65] and UV–vis spectroscopy were used to detect the redox intermediates during the redox reactions of QPT-OMe. The electrochemical EPR spectra shown in **Figure 5a** indicated radical signals both at oxidized and reduced states of QPT-OMe, and the spectra match well with simulated ones. [66,67] At the oxidized state, the spectrum exhibited three peaks with strong hyperfine coupling ($a \approx 0.65$ mT). This is attributed to the localized radical electron that distributes mainly around the N and S atoms in the phenothiazine moiety and extends to the entire conjugated structure, as revealed by the spin density distribution shown in **Figure 5b**. At the reduced state, the spectrum showed five peaks with an integration ratio of approximately 1:4:6:4:1 and a hyperfine coupling constant ($a \approx 0.36$ mT), which is due to the four spin resonance H atoms linking with the four carbon atoms in turquoise color (**Figure 5c**). Different from $QPT^{\bullet+}$-OMe, the radical electron in $QPT^{\bullet-}$-OMe distributes mainly in the conjugated plane of acridone skeleton, according to the spin density distribution simulation of radical ions (**Figure 5b-c**). The extended conjugation, particularly for $QPT^{\bullet-}$-OMe, might account for enhancing the stability of ketone radicals that are usually require inert-gas protection during cell operation to avoid nucleophilic attack and/or aeration-induced degradation by the coexisting species in the electrolyte, or the need of complicated molecular engineering method to protect the reactive center via steric hindrance and alike. [68]

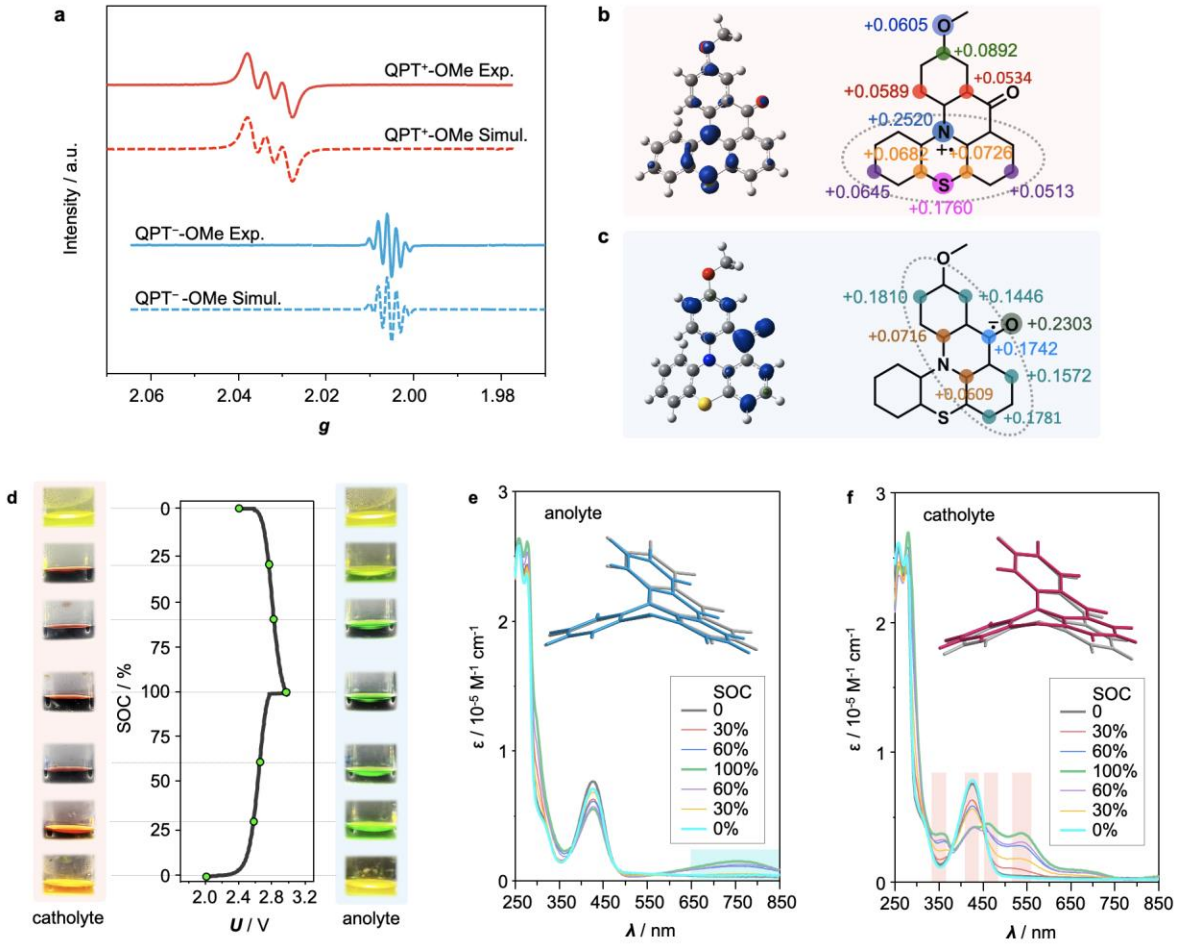

Figure 5. Spectroscopic study on structural variation of QPT-OMe during the electrochemical processes. a) Experimental and simulated EPR spectra of QPT$^{\bullet+}$-OMe and QPT$^{\bullet-}$-OMe; b) and c) spin density distribution of QPT$^{\bullet+}$-OMe and QPT$^{\bullet-}$-OMe. The panels on the left represent the visualized spin density that is in proportion to the distribution size, while the panels on the right give the calculated values on different atoms; d) Digital images showing the regular color change of the anolyte and catholyte at different SOCs of 0%, 30%, 60%, 100%, 60%, 30% and 0% in a complete charge-discharge cycle; e) and f) Corresponding UV-vis spectra at different SOCs. The molecule structure in the inset image indicated the structural distortion with respect to QPT-OMe sketched in grey.

The digital images shown in **Figure 5d** reveal that both the anolyte and catholyte showed strong and periodic color change during the oxidation and reduction processes. The color change can be directly

used to monitor the state-of-charge of a cell, avoiding the use of costly and complex battery management system. [69] As shown in **Figure 5e,** the UV–vis spectra of the anolyte showed no obvious change at the wavelength region below 500 nm during a charge/discharge cycle. A broad adsorption band gradually appeared at 650-850 nm when the state-of-charge (SOC) increased from 0% to 100%. For catholyte, the absorptivity around 425 nm slightly decreased when SOC increased, while the intensities of the bands at ca. 350, 470, and 540 nm increased (**Figure 5f**). And the reversible spectroscopic changes were observed during cycling indicated a decent stability and reversibility of electrochemical process. As known, new adsorption bands appear when energy difference between π and π^* orbitals of a conjugated structure decrease upon gaining additional negative or positive charge. [70,71] The appearance of new adsorption bands towards longer wavelength in **Figure 5e** is expected to be correlated to the structure distortion of QPT upon oxidation. The optimized structure of $QPT^{\bullet-}$ during the reduction process indicated a small distortion that mainly occurs on the acridone skeleton plane (inset of Figure 5e), whereas more obvious distortion was found in the entire conjugated structure during the oxidation process, and the phenothiazine moiety of $QPT^{\bullet+}$ tends to be more planar and thus have a better conjugation (inset of **Figure 5f**). The variations in the conjugation of $QPT^{\bullet+}$ and $QPT^{\bullet-}$ thus results in distinctly different UV-vis adsorption. In addition, nucleus-independent chemical shift (NICS) analysis (Figure S16) confirmed that the change of NICS values caused by structural distortion is mainly found in the heterocycle and the two attached hexatomic rings in QPT-OMe and more likely to delocalize throughout the entire conjugation in $QPT^{\bullet+}$-OMe. Based on the above analysis, the extended conjugation in the redox intermediates of QPT-OMe is advantageous in maintaining chemical stability compared with individual

quaternary N or ketone redox centers, suggesting the fused conjugation strategy not only provides a platform to develop new BRMs with broadened voltage gaps, but also endows the as-designed BRMs with enhanced stability compared with those using individual redox-active moieties. Further enhancement in solubility and voltage would be in turn by modifying the general formula with more soluble motifs and integrating other redox center with maximized redox potential.

In conclusion, a general strategy is proposed to develop new small bipolar molecules for symmetric RFBs to alleviate the major issue of electrolyte crossover. The strategy uses fused conjugation to regulate the electron density redistribution and further to regulate the redox potentials of the integrated redox-active moieties. A new bipolar molecule, QPT-OMe, based on a fused conjugation of quaternary N and ketone redox moiety is designed and used as the active material in a symmetric cell. The results showed that the fused conjugation can promote the electron density in the conjugation to redistribute from electron-deficient ketone moiety to electron-rich quaternary N moiety, resulting in the broadening of the voltage gap between the two redox moieties. Molecular geometry and spectroscopic analysis on the redox intermediates revealed that the negative charge on the reduced QPT-OMe is mainly delocalized in the heterocycle and the two attached hexatomic rings, while the positive charge on the oxidized QPT-OMe is more likely to delocalize throughout the entire conjugation. Applied as the sole active material in a symmetric cell, QPT-OMe delivered a cell voltage of 2.5 V, which is one of the highest cell voltages achieved in BRMs for symmetric RFBs so far, and maintained fast redox kinetics and decent cycling stability. The strategy proposed in this study may contribute to designing small-molecular-weight BRMs

that are essential to overcome the issues of electrolyte crossover and low cell voltage of RFBs, leading to enriched cell chemistry and simplified cell architecture.

Supporting Information

Details of experimental procedures and methods; synthetic routes (Scheme S1); DFT simulations results and summary of reported redox active materials in flow batteries (Tables S1−S2); additional discussion, characterization, DFT simulations and electrochemical analysis results (Figures S1−S16) (PDF)

Acknowledgments

Y.Z. and G.D. acknowledge the support from the National Natural Science Foundation of China (Grant Nos. 22179031, 22109111), the Natural Science Foundation of Zhejiang Province (Grant No LY22B030008, LQ22B030006), the Natural Science Foundation of the Jiangsu Higher Education Institutions of China (Grant No. 20KJB480002). Y.X. acknowledges the support from the Engineering and Physical Sciences Research Council (EP/V000152/1), the Leverhulme Trust (RPG-2021-138), and the Royal Society (RGS/R2/212324). X.Z. and Y.Z. acknowledge the support from the Collaborative Innovation Center of Suzhou Nano Science & Technology, the Priority Academic Program Development of Jiangsu Higher Education Institutions (PAPD), the 111 Project, and the Joint International Research Laboratory of Carbon-Based Functional Materials and Devices.

References

[1] Dunn, B.; Kamath, H.; Tarascon, J. M., Electrical energy storage for the grid: A battery of choices. *Science* **2011,** *334* (6058), 928-935.

[2] Yan, R.; Wang, Q., Redox-targeting-based flow batteries for large-scale energy storage. *Adv. Mater.* **2018,** *30* (47), 1802406.

[3] Soloveichik, G. L., Flow batteries: Current status and trends. *Chem. Rev.* **2015,** *115* (20), 11533-11558.

[4] Winsberg, J.; Hagemann, T.; Janoschka, T.; Hager, M. D.; Schubert, U. S., Redox-flow batteries: From metals to organic redox-active materials. *Angew. Chem. Int. Ed.* **2017,** *56* (3), 686-711.

[5] Luo, J.; Hu, B.; Hu, M.; Zhao, Y.; Liu, T. L., Status and prospects of organic redox flow batteries toward sustainable energy storage. *ACS Energy Lett.* **2019,** *4* (9), 2220-2240.

[6] Kwon, G.; Lee, S.; Hwang, J.; Shim, H.-S.; Lee, B.; Lee, M. H.; Ko, Y.; Jung, S.-K.; Ku, K.; Hong, J.; Kang, K., Multi-redox molecule for high-energy redox flow batteries. *Joule* **2018,** *2* (9), 1771-1782.

[7] Darling, R. M.; Gallagher, K. G.; Kowalski, J. A.; Ha, S.; Brushett, F. R., Pathways to low-cost electrochemical energy storage: A comparison of aqueous and nonaqueous flow batteries. *Energy Environ. Sci.* **2014,** *7* (11), 3459-3477.

[8] Milshtein, J. D.; Kaur, A. P.; Casselman, M. D.; Kowalski, J. A.; Modekrutti, S.; Zhang, P. L.; Harsha Attanayake, N.; Elliott, C. F.; Parkin, S. R.; Risko, C.; Brushett, F. R.; Odom, S. A., High

current density, long duration cycling of soluble organic active species for non-aqueous redox flow batteries. *Energy Environ. Sci.* **2016,** *9* (11), 3531-3543.

[9] Kwon, G.; Lee, K.; Lee, M. H.; Lee, B.; Lee, S.; Jung, S.-K.; Ku, K.; Kim, J.; Park, S. Y.; Kwon, J. E.; Kang, K., Bio-inspired Molecular Redesign of a Multi-redox Catholyte for High-Energy Non-aqueous Organic Redox Flow Batteries. *Chem* **2019,** *5* (10), 2642-2656.

[10] Ding, Y.; Zhang, C.; Zhang, L.; Zhou, Y.; Yu, G., Pathways to widespread applications: Development of redox flow batteries based on new chemistries. *Chem* **2019,** *5* (8), 1964-1987.

[11] Schon, T. B.; McAllister, B. T.; Li, P.-F.; Seferos, D. S., The rise of organic electrode materials for energy storage. *Chem. Soc. Rev.* **2016,** *45* (22), 6345-6404.

[12] Lee, S.; Hong, J.; Kang, K., Redox-active organic compounds for future sustainable energy storage system. *Adv. Energy Mater.* **2020,** *10* (30), 2001445.

[13] Ding, Y.; Zhang, C.; Zhang, L.; Zhou, Y.; Yu, G., Molecular engineering of organic electroactive materials for redox flow batteries. *Chem. Soc. Rev.* **2018,** *47* (1), 69-103.

[14] Perry, M. L.; Saraidaridis, J. D.; Darling, R. M., Crossover mitigation strategies for redox-flow batteries. *Curr. Opin. Electrochem.* **2020,** *21*, 311-318.

[15] Song, Z.; Zhou, H., Towards sustainable and versatile energy storage devices: an overview of organic electrode materials. *Energy Environ. Sci.* **2013,** *6* (8), 2280-2301.

[16] Duan, W.; Vemuri, R. S.; Milshtein, J. D.; Laramie, S.; Dmello, R. D.; Huang, J.; Zhang, L.; Hu, D.; Vijayakumar, M.; Wang, W.; Liu, J.; Darling, R. M.; Thompson, L.; Smith, K.; Moore, J. S.;

Brushett, F. R.; Wei, X., A symmetric organic-based nonaqueous redox flow battery and its state of charge diagnostics by FTIR. *J. Mater. Chem. A* **2016,** *4* (15), 5448-5456.

[17] Potash, R. A.; McKone, J. R.; Conte, S.; Abruña, H. D., On the benefits of a symmetric redox flow battery. *J. Electrochem. Soc.* **2016,** *163* (3), A338-A344.

[18] Lourenssen, K.; Williams, J.; Ahmadpour, F.; Clemmer, R.; Tasnim, S., Vanadium redox flow batteries: A comprehensive review. *J. Energy Storage* **2019,** *25* (7), 100844.

[19] Nambafu, G. S.; Siddharth, K.; Zhang, C.; Zhao, T.; Chen, Q.; Amine, K.; Shao, M., An organic bifunctional redox active material for symmetric aqueous redox flow battery. *Nano Energy* **2021,** *89*, 106422.

[20] Zhang, C.; Qian, Y.; Ding, Y.; Zhang, L.; Guo, X.; Zhao, Y.; Yu, G., Biredox eutectic electrolytes derived from organic redox-active molecules: High-energy storage systems. *Angew. Chem. Int. Ed.* **2019,** *58* (21), 7045-7050.

[21] Chen, H.; Niu, Z.; Zhao, Y., Redox-active binary eutectics: Preparation and their electrochemical properties. *Electrochem. Commun.* **2021,** *126*, 107028.

[22] Zhang, C.; Chen, H.; Qian, Y.; Dai, G.; Zhao, Y.; Yu, G., General design methodology for organic eutectic electrolytes toward high-energy-density redox flow batteries. *Adv. Mater.* **2021,** *33* (15), 2008560.

[23] Zhang, C.; Zhang, L.; Ding, Y.; Guo, X.; Yu, G., Eutectic electrolytes for high-energy-density redox flow batteries. *ACS Energy Lett.* **2018,** *3* (12), 2875-2883.

[24] Zhen, Y.; Zhang, C.; Yuan, J.; Zhao, Y.; Li, Y., Ferrocene/anthraquinone based bi-redox molecule for symmetric nonaqueous redox flow battery. *J. Power Sources* **2020,** *480* (7), 229132.

[25] Hwang, S.; Kim, H.-s.; Ryu, J. H.; Oh, S. M., N-ferrocenylphthalimide; A single redox couple formed by attaching a ferrocene moiety to phthalimide for non-aqueous flow batteries. *J. Power Sources* **2018,** *395* (5), 60-65.

[26] Zhu, Y.; Yang, F.; Niu, Z.; Wu, H.; He, Y.; Zhu, H.; Ye, J.; Zhao, Y.; Zhang, X., Enhanced cyclability of organic redox flow batteries enabled by an artificial bipolar molecule in neutral aqueous electrolyte. *J. Power Sources* **2019,** *417* (1), 83-89.

[27] Geysens, P.; Li, Y.; Vankelecom, I.; Fransaer, J.; Binnemans, K., Highly soluble 1,4-diaminoanthraquinone derivative for nonaqueous symmetric redox flow batteries. *ACS Sustainable Chem. Eng.* **2020,** *8* (9), 3832-3843.

[28] Wang, W.; Kim, S.; Chen, B.; Nie, Z.; Zhang, J.; Xia, G.-G.; Li, L.; Yang, Z., A new redox flow battery using Fe/V redox couples in chloride supporting electrolyte. *Energy Environ. Sci.* **2011,** *4* (10), 4068-4073.

[29] Duan, W.; Huang, J.; Kowalski, J. A.; Shkrob, I. A.; Vijayakumar, M.; Walter, E.; Pan, B.; Yang, Z.; Milshtein, J. D.; Li, B.; Liao, C.; Zhang, Z.; Wang, W.; Liu, J.; Moore, J. S.; Brushett, F. R.; Zhang, L.; Wei, X., "Wine-dark sea" in an organic flow battery: Storing negative charge in 2,1,3-benzothiadiazole radicals leads to improved cyclability. *ACS Energy Lett.* **2017,** *2* (5), 1156-1161.

[30] Barton, J. L.; Milshtein, J. D.; Hinricher, J. J.; Brushett, F. R., Quantifying the impact of viscosity on mass-transfer coefficients in redox flow batteries. *J. Power Sources* **2018,** *399* (7), 133-143.

[31] Zhang, C.; Zhang, L.; Ding, Y.; Peng, S.; Guo, X.; Zhao, Y.; He, G.; Yu, G., Progress and prospects of next-generation redox flow batteries. *Energy Storage Mater.* **2018,** *15* (6), 324-350.

[32] Sevov, C. S.; Brooner, R. E. M.; Chénard, E.; Assary, R. S.; Moore, J. S.; Rodríguez-López, J.; Sanford, M. S., Evolutionary Design of Low Molecular Weight Organic Anolyte Materials for Applications in Nonaqueous Redox Flow Batteries. *J. Am. Chem. Soc.* **2015,** *137* (45), 14465-14472.

[33] Wei, X.; Pan, W.; Duan, W.; Hollas, A.; Yang, Z.; Li, B.; Nie, Z.; Liu, J.; Reed, D.; Wang, W.; Sprenkle, V., Materials and systems for organic redox flow batteries: Status and challenges. *ACS Energy Lett.* **2017,** *2* (9), 2187-2204.

[34] Friedl, J.; Lebedeva, M. A.; Porfyrakis, K.; Stimming, U.; Chamberlain, T. W., All-fullerene-based cells for nonaqueous redox flow batteries. *J. Am. Chem. Soc.* **2018,** *140* (1), 401-405.

[35] Cao, J.; Tian, J.; Xu, J.; Wang, Y., Organic flow batteries: Recent progress and perspectives. *Energ. Fuel.* **2020,** *34* (11), 13384-13411.

[36] Li, M.; Case, J.; Minteer, S. D., Bipolar redox-active molecules in non-aqueous organic redox flow batteries: Status and challenges. *ChemElectroChem* **2021,** *8* (7), 1215-1232.

[37] Sikukuu Nambafu, G., Organic molecules as bifunctional electroactive materials for symmetric redox flow batteries: A mini review. *Electrochem. Commun.* **2021,** *127*, 107052.

[38] Zhang, L.; Qian, Y.; Feng, R.; Ding, Y.; Zu, X.; Zhang, C.; Guo, X.; Wang, W.; Yu, G., Reversible redox chemistry in azobenzene-based organic molecules for high-capacity and long-life nonaqueous redox flow batteries. *Nat. Commun.* **2020,** *11* (1), 3843.

[39] Ma, T.; Pan, Z.; Miao, L.; Chen, C.; Han, M.; Shang, Z.; Chen, J., Porphyrin-based symmetric redox-flow batteries towards cold-climate energy storage. *Angew. Chem. Int. Ed.* **2018,** *57* (12), 3158-3162.

[40] Qin, K.; Huang, J.; Holguin, K.; Luo, C., Recent advances in developing organic electrode materials for multivalent rechargeable batteries. *Energy Environ. Sci.* **2020,** *13* (11), 3950-3992.

[41] Zhao, Y.; Ding, Y.; Li, Y.; Peng, L.; Byon, H. R.; Goodenough, J. B.; Yu, G., A chemistry and material perspective on lithium redox flow batteries towards high-density electrical energy storage. *Chem. Soc. Rev.* **2015,** *44* (22), 7968-7996.

[42] Kim, J.; Kim, H.; Lee, S.; Kwon, G.; Kang, T.; Park, H.; Tamwattana, O.; Ko, Y.; Lee, D.; Kang, K., A p-n fusion strategy to design bipolar organic materials for high-energy-density symmetric batteries. *J. Mater. Chem. A* **2021,** *9* (25), 14485-14494.

[43] Kwon, G.; Lee, K.; Yoo, J.; Lee, S.; Kim, J.; Kim, Y.; Kwon, J. E.; Park, S. Y.; Kang, K., Highly persistent triphenylamine-based catholyte for durable organic redox flow batteries. *Energy Storage Mater.* **2021,** *42*, 185-192.

[44] Dai, G.; Liu, Y.; Niu, Z.; He, P.; Zhao, Y.; Zhang, X.; Zhou, H., The design of quaternary nitrogen redox center for high-performance organic battery materials. *Matter* **2019,** *1* (4), 945-958.

[45] Dai, G.; Wu, T.; Chen, H.; Zhao, Y., Quaternary nitrogen redox centers for battery materials. *Curr. Opin. Electrochem.* **2021,** *29*, 100745.

[46] Ding, Y.; Zhang, C.; Zhang, L.; Wei, H.; Li, Y.; Yu, G., Insights into hydrotropic solubilization for hybrid ion redox flow batteries. *ACS Energy Lett.* **2018,** *3* (11), 2641-2648.

[47] Reed, A. E.; Weinhold, F., Natural localized molecular orbitals. *J. Chem. Phys.* **1985,** *83* (4), 1736-1740.

[48] Zhang, F.; Cheng, Y.; Niu, Z.; Ye, J.; Dai, G.; Zhang, X.; Zhao, Y., Tailoring the voltage gap of organic battery materials based on a multi-electron redox chemistry. *ChemElectroChem* **2020,** *7* (7), 1781-1788.

[49] Simon, P.; Gogotsi, Y.; Dunn, B., Where do batteries end and supercapacitors begin? *Science* **2014,** *343* (6176), 1210-1211.

[50] Nicholson, R. S., Theory and application of cyclic voltammetry for measurement of electrode reaction kinetics. *Anal. Chem.* **1965,** *37* (11), 1351-1355.

[51] Wang, H.; Sayed, S. Y.; Luber, E. J.; Olsen, B. C.; Shirurkar, S. M.; Venkatakrishnan, S.; Tefashe, U. M.; Farquhar, A. K.; Smotkin, E. S.; McCreery, R. L.; Buriak, J. M., Redox flow batteries: How to determine electrochemical kinetic parameters. *ACS Nano* **2020,** *14* (3), 2575-2584.

[52] Li, M.; Rhodes, Z.; Cabrera-Pardo, J. R.; Minteer, S. D., Recent advancements in rational design of non-aqueous organic redox flow batteries. *Sustainable Energy & Fuels* **2020,** *4* (9), 4370-4389.

[53] Mikhaylik, Y. V.; Akridge, J. R., Polysulfide shuttle study in the Li/S battery system. *J. Electrochem. Soc.* **2004,** *151* (11), A1969-A1976.

[54] Wei, X.; Xu, W.; Huang, J.; Zhang, L.; Walter, E.; Lawrence, C.; Vijayakumar, M.; Henderson, W. A.; Liu, T.; Cosimbescu, L.; Li, B.; Sprenkle, V.; Wang, W. Radical Compatibility with nonaqueous electrolytes and its impact on an all-organic redox flow battery. Angew. Chemie Int. Ed. 2015, 54 (30), 8684-8687.

[55] Wei, X.; Duan, W.; Huang, J.; Zhang, L.; Li, B.; Reed, D.; Xu, W.; Sprenkle, V.; Wang, W. A high-current, stable nonaqueous organic redox flow battery. ACS Energy Lett. 2016, 1 (4), 705-711.

[56] Lin, K.; Chen, Q.; Gerhardt, M. R.; Tong, L.; Kim, S. B.; Eisenach, L.; Valle, A. W.; Hardee, D.; Gordon, R. G.; Aziz, M. J.; Marshak, M. P., Alkaline quinone flow battery. *Science* **2015,** *349* (6255), 1529-1532.

[57] Yuan, J.; Zhang, C.; Zhen, Y.; Zhao, Y.; Li, Y., Enhancing the performance of an all-organic non-aqueous redox flow battery. *J. Power Sources* **2019,** *443* (6), 227283.

[58] Jin, S.; Jing, Y.; Kwabi, D. G.; Ji, Y.; Tong, L.; De Porcellinis, D.; Goulet, M.-A.; Pollack, D. A.; Gordon, R. G.; Aziz, M. J., A water-miscible quinone flow battery with high volumetric capacity and energy density. *ACS Energy Lett.* **2019,** *4* (6), 1342-1348.

[59] Shkrob, I. A.; Robertson, L. A.; Yu, Z.; Assary, R. S.; Cheng, L.; Zhang, L.; Sarnello, E.; Liu, X.; Li, T.; Preet Kaur, A.; Malsha Suduwella, T.; Odom, S. A.; Wang, Y.; Ewoldt, R. H.; Farag, H. M.; Z, Y., Crowded electrolytes containing redoxmers in different states of charge: Solution structure, properties, and fundamental limits on energy density. *J. Mol. Liq.* **2021,** *334*, 116533.

[60] Chen, H.; Cong, G.; Lu, Y.-C., Recent progress in organic redox flow batteries: Active materials, electrolytes and membranes. *J. Energy Chem.* **2018,** *27* (5), 1304-1325.

[61] Winsberg, J.; Stolze, C.; Muench, S.; Liedl, F.; Hager, M. D.; Schubert, U. S., TEMPO/phenazine combi-molecule: A redox-active material for symmetric aqueous redox-flow batteries. *ACS Energy Lett.* **2016,** *1* (5), 976-980.

[62] Hwang, S.; Kim, H.-s.; Ryu, J. H.; Oh, S. M., N-(α-ferrocenyl)ethylphthalimide as a single redox couple for non-aqueous flow batteries. *J. Power Sources* **2019,** *421*, 1-5.

[63] Hagemann, T.; Winsberg, J.; Häupler, B.; Janoschka, T.; Gruber, J. J.; Wild, A.; Schubert, U. S., A bipolar nitronyl nitroxide small molecule for an all-organic symmetric redox-flow battery. *NPG Asia Materials* **2017,** *9* (1), e340.

[64] Moutet, J.; Veleta, J. M.; Gianetti, T. L., Symmetric, robust, and high-voltage organic redox flow battery model based on a helical carbenium ion electrolyte. *ACS Appl. Energy Mater.* **2021,** *4* (1), 9-14.

[65] Murray, P. R.; Collison, D.; Daff, S.; Austin, N.; Edge, R.; Flynn, B. W.; Jack, L.; Leroux, F.; McInnes, E. J. L.; Murray, A. F.; Sells, D.; Stevenson, T.; Wolowska, J.; Yellowlees, L. J. An in situ electrochemical cell for Q- and W-Band EPR spectroscopy. J. Magn. Reson. 2011, 213 (1), 206–209.

[66] Mao, L.; Zhou, M.; Niu, Y.-F.; Zhao, X.-L.; Shi, X., Aryl carbazole-based macrocycles: Synthesis, their remarkably stable radical cations and host-guest complexation with fullerenes. *Org. Chem. Front.* **2021,** *8* (17), 4678-4684.

[67] Huo, G.-F.; Shi, X.; Tu, Q.; Hu, Y.-X.; Wu, G.-Y.; Yin, G.-Q.; Li, X.; Xu, L.; Ding, H.-M.; Yang, H.-B., Radical-induced hierarchical self-assembly involving supramolecular coordination complexes in both solution and solid states. *J. Am. Chem. Soc.* **2019,** *141* (40), 16014-16023.

[68] Zhu, Y.; Li, Y.; Qian, Y.; Zhang, L.; Ye, J.; Zhang, X.; Zhao, Y., Anthraquinone-based anode material for aqueous redox flow batteries operating in nondemanding atmosphere. *J. Power Sources* **2021,** *501* (4), 229984.

[69] Skyllas-Kazacos, M.; Kazacos, M., State of charge monitoring methods for vanadium redox flow battery control. *J. Power Sources* **2011,** *196* (20), 8822-8827.

[70] Amthor, S.; Noller, B.; Lambert, C., UV/Vis/NIR spectral properties of triarylamines and their corresponding radical cations. *Chem. Phys.* **2005,** *316* (1-3), 141-152.

[71] Brédas, J.-L.; Beljonne, D.; Coropceanu, V.; Cornil, J., Charge-transfer and energy-transfer processes in π-conjugated oligomers and polymers: A molecular picture. *Chem. Rev.* **2004,** *104* (11), 4971-5004.